



LAWRENCE
LIVERMORE
NATIONAL
LABORATORY

Composite Amplitude Modulated Phase Only Filter Based Detection and Tracking of the Back-Reflection of KDP Images

A. A. S. Awwal, W. A. McClay, S. W. Ferguson, J.
V. Candy, J. T. Salmon, P. J. Wegner

September 22, 2004

SPIE 49th Annual Meeting
Denver, CO, United States
August 2, 2004 through August 6, 2004

Disclaimer

This document was prepared as an account of work sponsored by an agency of the United States Government. Neither the United States Government nor the University of California nor any of their employees, makes any warranty, express or implied, or assumes any legal liability or responsibility for the accuracy, completeness, or usefulness of any information, apparatus, product, or process disclosed, or represents that its use would not infringe privately owned rights. Reference herein to any specific commercial product, process, or service by trade name, trademark, manufacturer, or otherwise, does not necessarily constitute or imply its endorsement, recommendation, or favoring by the United States Government or the University of California. The views and opinions of authors expressed herein do not necessarily state or reflect those of the United States Government or the University of California, and shall not be used for advertising or product endorsement purposes.

Composite Amplitude Modulated Phase Only Filter Based Detection and Tracking of the Back-Reflection of KDP Images

Abdul Awwal, Wilbert McClay, Walter Ferguson, James Candy, Thad Salmon, and Paul Wegner
National Ignition Facility
University of California, Lawrence Livermore National Laboratory, Livermore, CA. 94551
E-mail: awwal1@llnl.gov

ABSTRACT

An algorithm for determining the position of the KDP back-reflection image was developed. It was compared to a centroid-based algorithm. While the algorithm based on centroiding exhibited a radial standard deviation of 9 pixels, the newly proposed algorithm based on classical matched filtering (CMF) and a Gaussian fit to correlation peak provided a radial standard deviation of less than 1 pixel. The speed of the peak detection was improved from an average of 5.5 seconds for Gaussian fit to 0.022 seconds by using a polynomial fit. The performance was enhanced even further by utilizing a composite amplitude modulated phase only filter; producing a radial standard deviation of 0.27 pixels. The proposed technique was evaluated on 900+ images with varying degrees of noise and image amplitude as well as real National Ignition Facility (NIF) images.

Key words: pattern recognition, matched filtering, amplitude modulated phase only filter, target tracking, optical alignment, automated optical alignment, centroid, KDP, NIF

1. INTRODUCTION

The National Ignition Facility, currently under construction at the Lawrence Livermore National Laboratory, is a stadium-sized facility containing a 192-beam, 1.8-megajoule, 500-terawatt, ultraviolet laser system for the study of inertial confinement fusion and the physics of matter at extreme energy densities and pressures [1]. Automatic alignment is one of the most important operations on NIF, which requires high accuracy and fault tolerance. At the heart of this technique is the beam position detection algorithm. Before reaching the target chamber the beam must pass through a potassium dihydrogen phosphate (KDP) crystal.

The beam alignment is performed using the reflection from the back surface of the crystal. The determination of the position of the KDP back-reflection beam has been a long-standing challenge for the automatic alignment of the KDP crystals at NIF. The KDP crystals act as a frequency converter to harmonically convert the infrared laser light to ultraviolet. They produce maximum gain for a certain tilt angle. This angular tilt must be determined from the position of the back-reflection of the frequency conversion crystals. The KDP crystal angle must be adjusted within ± 20 μ rad over a field of view of ± 200 μ rad. Due to gravity and other effects, the KDP crystals exhibit a sag, which introduces a phase aberration into the beam. As a result, the beam reflected from the second KDP surface suffers phase distortion, and produces a diamond shaped beam pattern. The challenge was to find a stable measurement of the beam position, which should remain stable if no mechanical movement of the crystal occurs.

A *weighted centroid* was used to determine the position of the back-reflection. However, due to local intensity variation termed “boiling noise” the weighted centroid position varied significantly from frame to frame. To overcome this problem, a *binary centroid* was used. It was expected that binarization would hide the variation of intensity. However, since binarization is a function of the threshold value used to binarize the image, as the image intensity varies the centroid position varies by 8 or more pixels in any one direction. Thus an alternate algorithm such as a matched filter is sought.

One of the characteristics of the KDP back-reflection image is the presence of well-defined, relatively stable fringe patterns within the beam. We show in this paper that these fringe patterns facilitate a stable beam position detection method based on a composite [2] *amplitude modulated phase only matched filter* (AMPOF) [3].

2. ALGORITHM DESCRIPTION

VanderLugt was the first to introduce the *classical matched filter* (CMF) for optical pattern recognition [4]. In this method, the complex amplitude and phase of the reference pattern is stored as a hologram. The *phase only filter* (POF) is a variation of the CMF, which uses only the phase of the reference pattern to perform correlation detection [5]. The AMPOF was designed to further enhance the performance of the POF [3]. The mathematical foundation of the AMPOF filter is derived as shown in the following equations. Let the Fourier transform of the object function $f(x,y)$ be denoted by:

$$F(U_x, U_y) = |F(U_x, U_y)| \exp(j\Phi(U_x, U_y)) \quad (1)$$

Then a CMF corresponding to this function $f(x,y)$ is expected to produce its autocorrelation. From the Fourier transform theory of correlation, the CMF is given by the complex conjugate of the input Fourier spectrum as denoted by Equation 2.

$$H_{CMF}(U_x, U_y) = F^*(U_x, U_y) = |F(U_x, U_y)| \exp(-j\Phi(U_x, U_y)) \quad (2)$$

The inverse Fourier transformation of the product of $F(U_x, U_y)$ and $H_{CMF}(U_x, U_y)$ results in the convolution of $f(x, y)$ and $f(-x, -y)$, which is the equivalent of the autocorrelation of $f(x, y)$. Moreover, when $|F(U_x, U_y)|$ is set to unity, H_{CMF} becomes a *phase only filter* (POF) as shown in Equation 3.

$$H_{POF}(U_x, U_y) = \exp(-j\Phi(U_x, U_y)) \quad (3)$$

Since the convolution operator in the space domain is equivalent to the product operator in the frequency domain, one can think of the POF as an edge enhancer by way of division by $|F(U_x, U_y)|$. To get an even sharper peak, it is useful to divide the H_{POF} by a magnitude function, which will lead to an impulse type of correlation. An AMPOF attempts to achieve exactly this. The generalized AMPOF filter is expressed as [6]:

$$H_{AMPOF}(U_x, U_y) = \frac{aF^*(U_x, U_y)}{[b + c|F(U_x, U_y)| + d|F(U_x, U_y)|^2]^m} \quad (4)$$

When, $a = b = m = 1$, $c = d = 0$, this results in the classical matched filter; when $b = d = 0$, $a = c$, $m = 1$ it results in a phase only filter expressed by Equation 3. When b is a small constant for nonzero values of a , c , and d it is an AMPOF. The AMPOF described in [3] has $a = \text{constant}$, $d = \text{constant}$, $c = 0$, $m = 1$ and $b = \epsilon$ (a small constant number). It was found, after some experimentation, that when $b = \epsilon$, $d = 0$ and $c = a = 1$, better stability of position detection results in the

current KDP beam. More detailed optimization of these parameters is possible [7,8]. The AMPOF correlation of the input image and the target is simply:

$$C_{AMPOF}(\Delta_x, \Delta_y) = F^{-1}\{F(U_x, U_y)H_{AMPOF}(U_x, U_y)\} \quad (5)$$

Samples of KDP beam reflections for four separate beam-lines are shown in Figure 1.

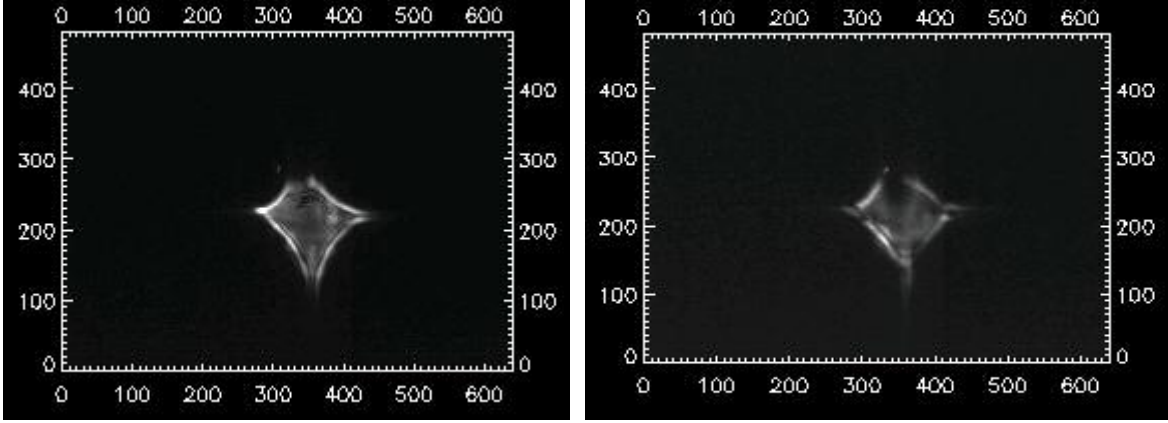


Figure 1. Example of real KDP back-reflection pattern

From Figure 1, it can be observed that the beams have significant variation among one another. Initially, we employed CMF to detect the KDP pattern. One of the images was selected as the template image. The position of this single image was determined off-line, by careful filtering and determining its weighted centroid. From the physics-based simulation of the KDP back-reflection, it is known that the position of the beam should be its weighted centroid if the camera has an infinite dynamic range [9]. In other words, in the absence of the phase distortion caused by the KDP crystal, the beam will converge to the weighted centroid of the back-reflection caused by the KDP crystals. Thus, if we know the original position of the KDP template, then by knowing the displacement from the current position we can calculate its new absolute position. By knowing the position of the correlation peak, we can also determine the relative displacement of the KDP beam with respect to its current position by subtracting the position of the autocorrelation peak for the template. Let the position of the original reference KDP beam be (x_c, y_c) . Then the position of the KDP after matched filtering is given by:

$$x_{pos} = x_{cross} - x_{auto} + x_c \quad (6)$$

$$y_{pos} = y_{cross} - y_{auto} + y_c \quad (7)$$

Where (x_{pos}, y_{pos}) is the position of the KDP, (x_{auto}, y_{auto}) is the position of the template autocorrelation peaks, and (x_{cross}, y_{cross}) is the position of the cross-correlation peak. The position of the cross-correlation peak was determined using a Gaussian fit to the correlation peak. The center of the template, (x_c, y_c) , is calculated off-line by a weighted centroid

approach. The position of the autocorrelation peak is also determined off-line. Both of these parameters are constants for the algorithm. They will only change if the templates are modified.

3. ALGORITHM TESTING AND MODIFICATIONS

In this section, we describe a series of experiments demonstrating the development of the AMPOF-based position detection scheme as well as gradual improvements to the algorithm. It is also compared to the existing centroid-based algorithm. The first experiment was performed using the classical matched filter over a set of 5 images (where the image was recorded in one position with consecutive frames). The centroid position obtained from previous binary centroid algorithms and the correlation peak obtained using matched filtering for comparison is shown in Table 1. Note that only the cross-correlation peak is recorded here since we are mainly interested in the stability of the measurement. The other parameters in Equations 6 and 7 remain constant. Note that the peak detection in this case was performed by a Gaussian fit to the correlation peak. From these tabular values the radial standard deviation is estimated for both cases. For the centroid-based case, the image in the same location but taken at different times shows wide variations of the position data, while the CMF case demonstrates a more stable measurement.

The radial standard deviation for CMF based detection is 0.99 pixels. This precision was a significant improvement over the previous binary centroid-based beam locator, which yielded a radial standard deviation of 9.1 pixels.

Table 1. The Output of the Centroiding and CMF Algorithm

Image	x-centroid	y-centroid	Correlation x-peak	Correlation y-peak	Comment
B315_KDP1_060903.tif	335.66	161.31	320.00	240.000	Auto correlation
B315_KDP2_060903.tif	328.085	152.554	320.435	238.022	Cross-peak
B315_KDP3_060903.tif	344.669	168.435	321.037	238.232	Cross-peak
B315_KDP4_060903.tif	336.907	161.298	319.963	239.129	Cross-peak
B315_KDP5_060903.tif	342.090	167.964	320.680	239.709	Cross-peak

One of the problems of the Gaussian fit algorithm is that it is computationally slow, consuming close to 3 seconds to execute. For real-time operation a faster method is preferred. A second order curve fit to the peak results in the following expression for the correlation peak positions:

$$X_{cross} = \frac{0.5f_0(x_1 + x_2) + 0.5f_2(x_0 + x_1) - 0.5f_1(x_0 + x_2)}{f_0 - 2f_1 + f_2} \quad (8)$$

Where the (x_i, f_i) pair represents the x position versus the intensity pairs. When the pair is replaced by the (y_i, f_i) pairs, it results in the corresponding y-locations.

$$Y_{cross} = \frac{0.5f_0(y_1 + y_2) + 0.5f_2(y_0 + y_1) - 0.5f_1(y_0 + y_2)}{f_0 - 2f_1 + f_2} \quad (9)$$

The pair (x_1, y_1) is the position of the peak intensity. A polynomial curve fit could be done in 0.02 seconds, which is approximately 240 times faster than a Gaussian curve fit. Surprisingly, the radial standard deviation improves to 0.60 pixels. Note that the first frame was used as the template for the consecutive frame images. Next, a composite filter was constructed from a weighted addition of three images. This filter further improved the deviation to 0.51 pixels.

An AMPOF correlation peak matches the texture of the image more closely, which results in a sharper correlation peak than any other filter, including the phase-only filter, and hopefully less radial standard deviation. A CMF correlation peak usually has a broad peak, but the correlation peak is smoother. Moving to an AMPOF performed further optimization on the composite CMF. Optimization was improved even further by developing a composite AMPOF filter [2,3] producing a radial standard deviation of only 0.27 pixels.

One reason why CMF shows a higher variance can be better understood by analyzing the correlation operation in the Fourier domain. For CMF, the correlation operation requires a squaring of the image magnitude and cancellation of the phase. Therefore, the correlation spot is the DC level of the cross product. The squaring introduces higher frequencies, thus taking energy away from the zero frequency. This also results in a smoother (opposite of a sharp peak) correlation peak that shows high variability. Figure 2 illustrates the sharpness of the AMPOF correlation peak as compared to that of a CMF. Thus a sharper correlation peak reduces the uncertainty number (0.9 pixels for CMF) by using an AMPOF filter.

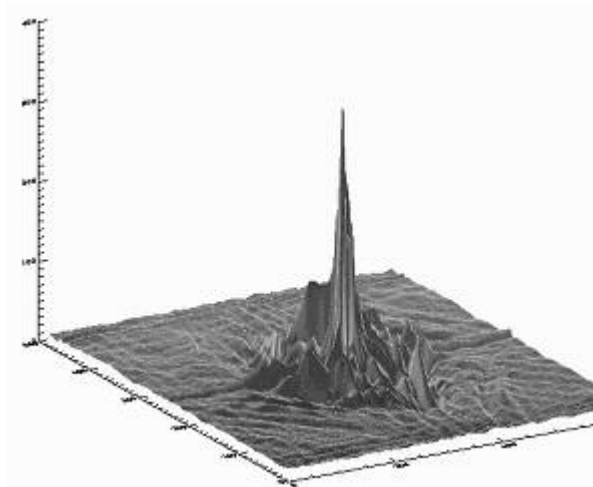
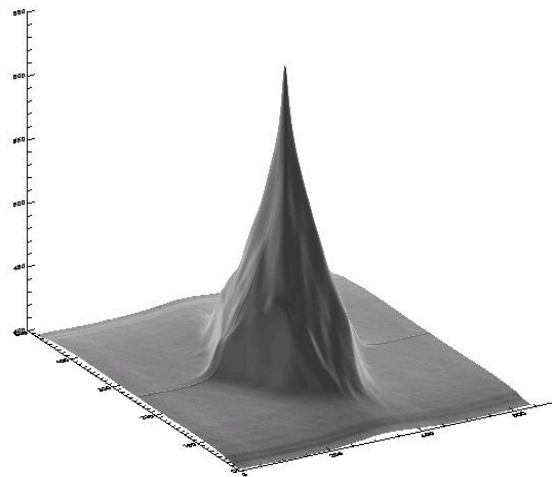


Figure 2(a). An AMPOF correlation peak



(b). A CMF peak has a broad base

Table 2. The Output of the Composite AMPOF Algorithm

Image	Correlation Plane		Image Plane		Comments
	x-peak	y-peak	x-centroid	y-centroid	
B315_KDP1_060903.tif	319.968	240.081	344.25	205.674	Auto correlation
B315_KDP2_060903.tif	319.948	239.986	344.518	205.583	Cross-peak
B315_KDP3_060903.tif	320.112	239.945	344.394	205.542	Cross-peak
B315_KDP4_060903.tif	319.505	239.796	343.787	205.393	Cross-peak
B315_KDP5_060903.tif	319.742	240.114	344.024	205.711	Cross-peak

4. STATISTICAL RESULTS WITH SIMULATED NOISE IMAGE SETS

In this section, we describe a method of calculating the uncertainty of this newly developed algorithm. An image of the real KDP back-reflection is recorded by manually segmenting its bright region. Now the amplitude of this image is scaled to 200, 100, and 50 to create examples of bright and dim images. Thereafter, white Gaussian noise is added with an rms count of 10, 20, and 50. We create a set of 100 images for each amplitude and rms noise. Then the algorithm is used to evaluate these images for each noise level and the standard deviation (one-sigma) of the position data is calculated. The three-sigma is taken as a measure of uncertainty. (It should be cautioned, however, this three-sigma does not guarantee a 99.875% probability of being correct. To calculate uncertainty using a probability approach one needs to fit the distribution and then to evaluate the range.)

The new algorithm was evaluated using 900 simulated noisy images as described above. Four samples from this set are shown in Figures 3-6. Its performance was compared to that of the existing algorithm currently operating at the NIF facility. The three-sigma uncertainty curves of these two runs are shown in Figures 7(a) and (b). The centroid based algorithm produces an uncertainty of 17 pixels, with maximum image amplitude 100 and noise rms of 50; the new algorithm produces uncertainty below 0.5 pixels for the same imaging condition as shown in the Figures 7(a) and (b). For these tests, the template was chosen from the undistorted image. From the curve for the standard case of amplitude 200 and noise count of 20, the three-sigma noise is less than 0.1 pixels. It should be noted that we used a single image to derive our template image and it does not incorporate any variations due to boiling noise. It is possible to use multiple images to incorporate image variability and improve the three-sigma range to an even lower value.

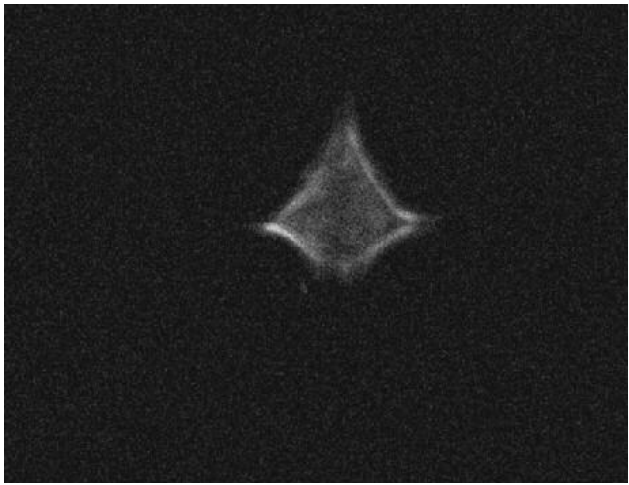


Figure 3. Amplitude max 200, noise 20 rms

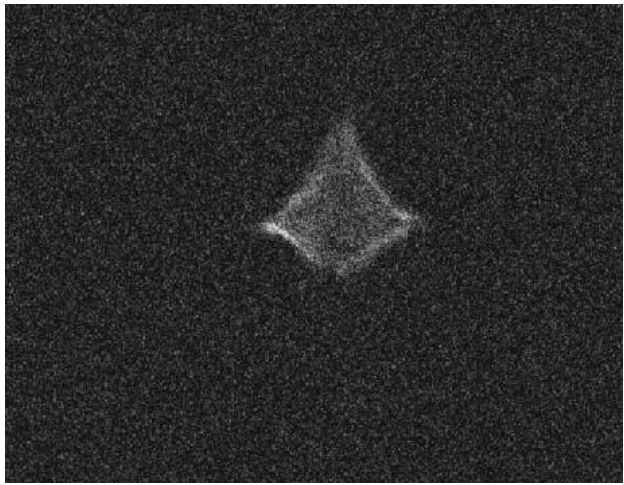


Figure 4. Amplitude max 200, noise 50 rms



Figure 5. Amplitude 200, interference 20, period λ

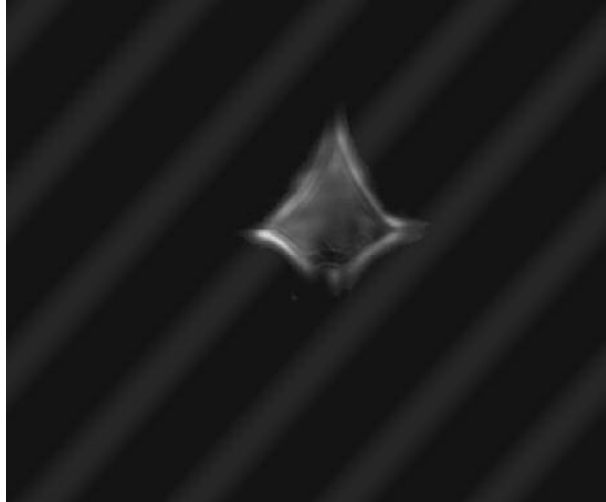


Figure 6. Amplitude 200, interference 20, period $\lambda/2$

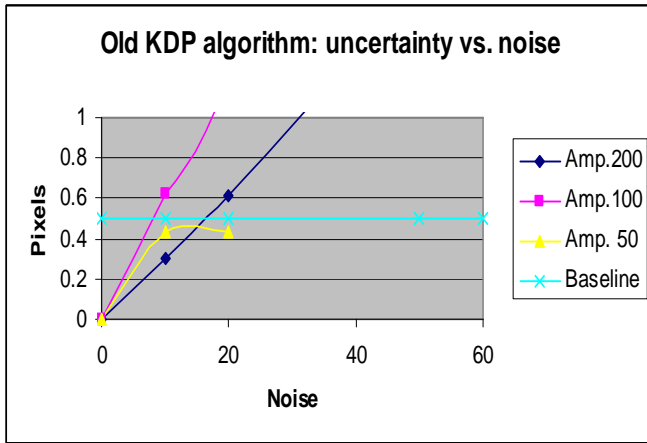
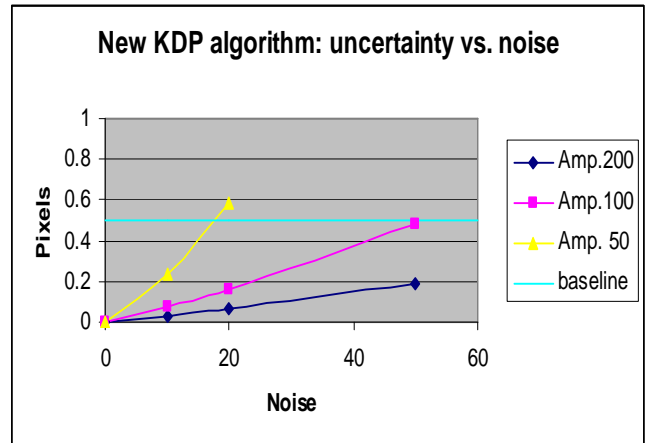


Figure 7(a). Noise versus uncertainty of centroid-based algorithm; noise in rms count and uncertainty in pixels



(b). Noise vs. uncertainty of the AMPOF algorithm

One problem with a real KDP image is that the absolute position is not really known. In order to evaluate the algorithm performance in terms of absolute location versus measured location, another set of 900 images was created from the original shown in Figure 8(a). Note that this image is artificially created, where the center location is either known or can be measured very accurately. Both Gaussian noise and diffraction noise were added to this image. Examples of diffraction pattern added images are shown in Figures 8(b) and 9.

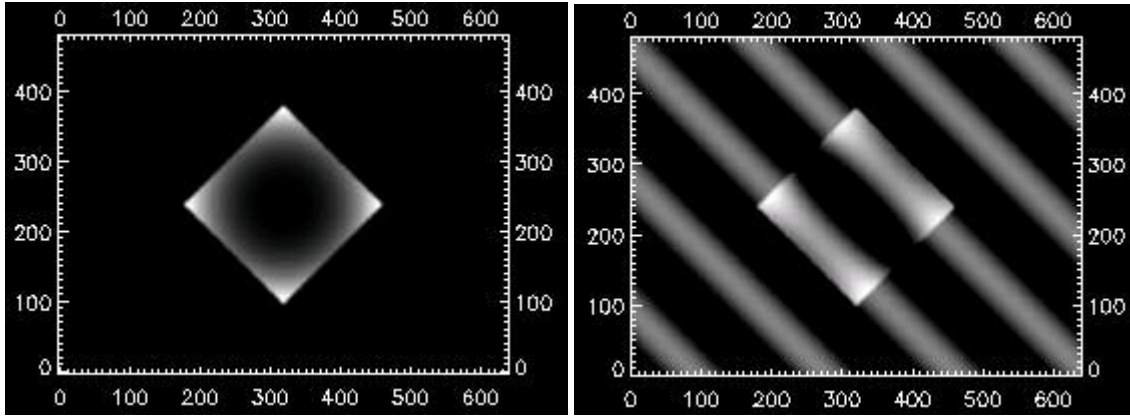


Figure 8(a). The original image

(b). Amplitude 100, interference amp. 50, 2 wave

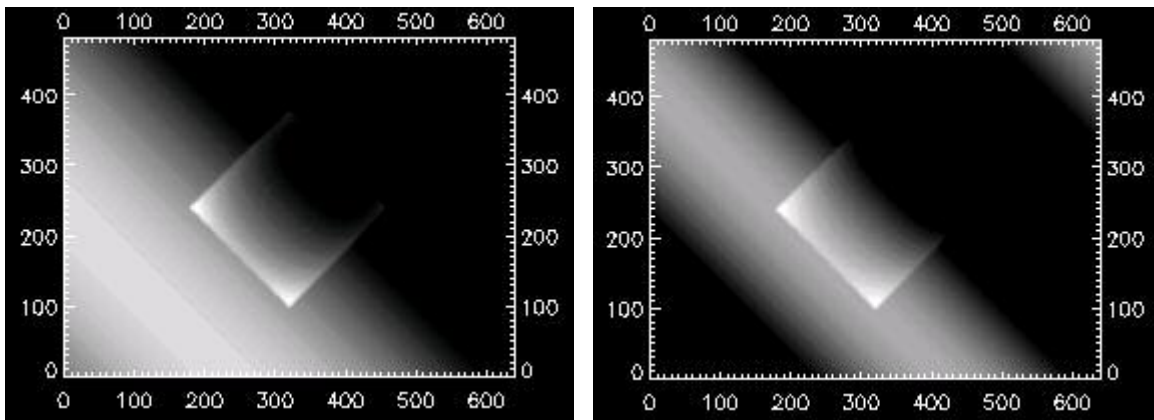


Figure 9(a). Amplitude 50, interference amplitude 50,

(b). Amplitude 50, interference amplitude 50, half-wave

The AMPOF filter was designed from the original image as shown in Figure 8(a). Interestingly, the interference noise images shown in Figures 9(a–b) illustrate that in some cases 50% of the image is missing. The results with these simulated KDP images are presented in Figures 10 and 11.

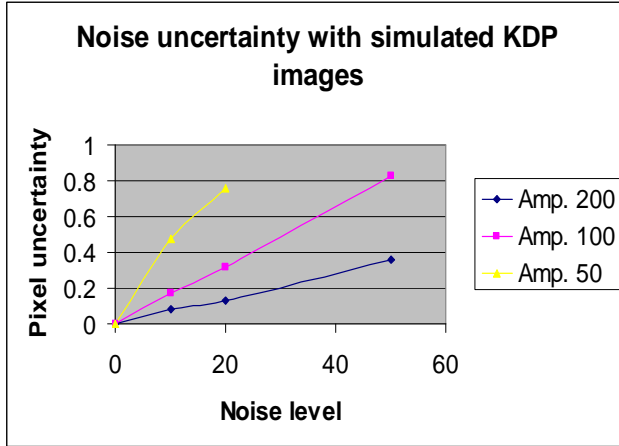
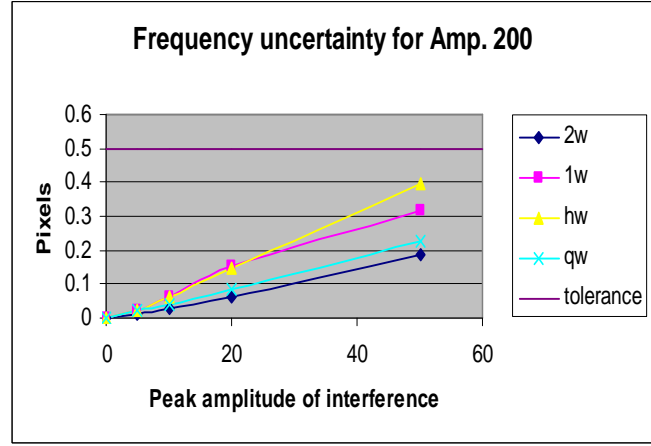


Figure 10(a). Noise versus uncertainty with new algorithm for various amplitude signal and rms noise



(b). Noise uncertainty for various wave distortions for various amplitudes of wave

From Figure 10(a) the amplitude 200 and 100 images with less than or equal to 20 count rms noise show an uncertainty less than the tolerance limit of 0.5 pixels. The results from images corrupted by interference type noise are shown in Figures 10(b) and 14.

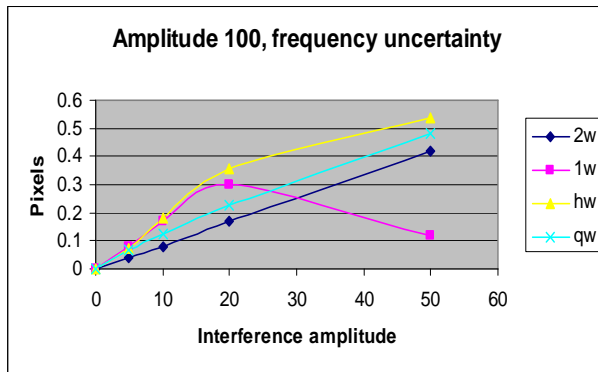
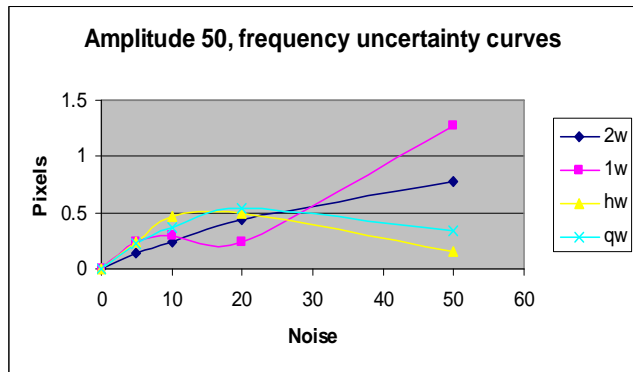


Figure 11(a). Noise versus uncertainty with new algorithm for various amplitude signal and rms noise



(b). Noise uncertainty for various wave distortions for various amplitudes of wave

Since in this experiment the true centroid position is known with a high degree of accuracy (no noise image), this position was used to calculate the difference between the average of position readings for each set and the true position. They were found to be bounded by the theoretical maximum of $3\sigma/\sqrt{n}$, where σ is the standard deviation of each set [10]. Even for the worst case where the signal amplitude was low and noise amplitude high, the actual deviation was found to be close to 0.1 as shown in Figure 12(a). The result can also be visualized in the accompanying scatter plot of a specific set in Figure 12(b).

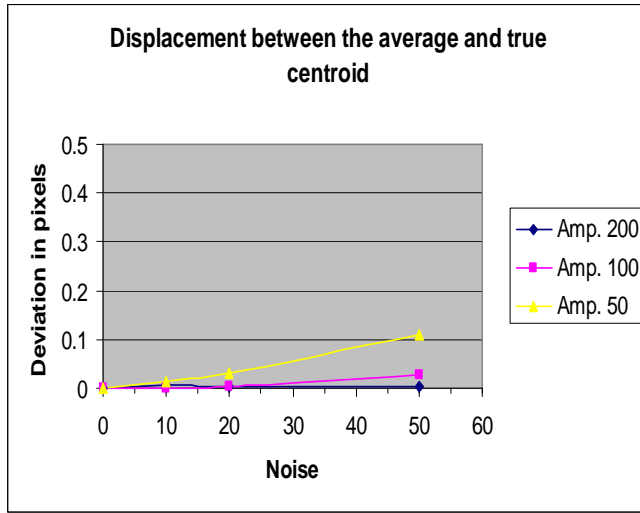
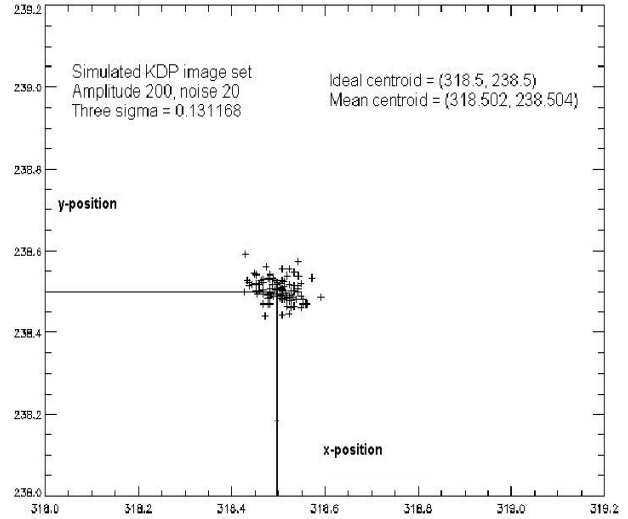


Figure 12(a). Displacement between the average and true centroids for various signal amplitude signal and rms noise



(b). Scatter plot for amplitude 200 with rms noise 20 count

One application of the uncertainty curves is to approximate the uncertainty from the real image. Estimating the noise rms of the image and then using the curves in Figure 10(a) as a lookup table and estimating the uncertainty from the closest interval containing the rms noise count accomplishes this. This allows us to ascertain that the error allowed for the alignment loop is within the error tolerance assigned in the total NIF error budget.

5. TEMPLATE FORMATION AND POST-PROCESSING

Since the KDP back-reflection images vary with time, the templates should be designed from a series of images, so that the variability is accommodated in the template. The filters were designed by averaging the real KDP images that remained within a two-sigma bound [11].

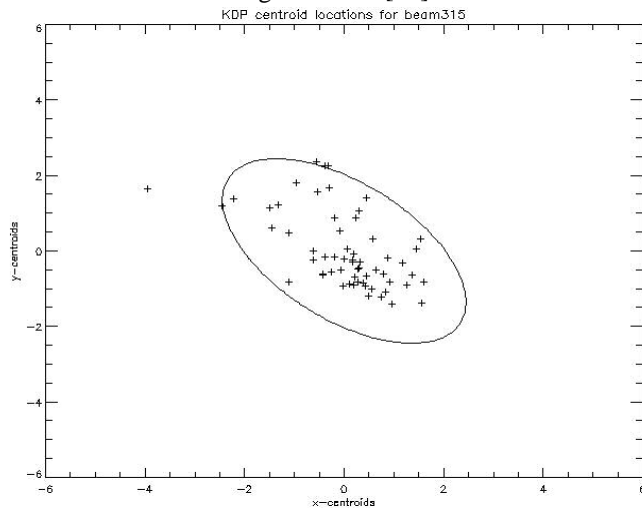


Figure 13. Scatter plot of 49 images taken over six months

The purpose of post-processing is to decide once an image has been processed if there is a certain probability that the image may be a wrong or different class of image. Thus, post-processing will eliminate any unreasonable results. The preprocessing usually eliminates simple cases of all dark, dim, or all white images. However, if these images are not rejected by the preprocessing stage then the post-processing will attempt to eliminate those cases. It is possible to derive post-processing based on different criteria such as correlation amplitude, normalized correlation peak, average energy correlation peak, average amplitude correlation peak, pedestal of the correlation peak (under half power points, 90% power points, etc.). We experimented with all of these possible parameters. The most promising was based on determining the pedestal under half power point.

Since we are using an AMPOF filter it produces a very sharp correlation peak. When the image contains high noise counts, multiple targets, and a background or white image; the number of peaks (which are mostly false) increases; as a result the pedestal count increases. The difficulty in normalizing images with saturated pixels prohibits us from using correlation peak magnitude. Table 3 illustrates the pedestal results:

Table 3. Width of Correlation Peak for Post-Processing

Beam number	Autocorrelation pedestal-in class (70.7% of maximum)	Cross-correlation Pedestal-out of class (70.7% of maximum)	Comments
B315	53		Low pedestal for noise free image
B315_2		194	Different beam-line image
B315_3		524	Different beam-line image
B315_4		193	Different beam-line image
a100_i20_hw	115		B315 interference noise 20
a100_n50	62		B315 amplitude 100 noise 50
a200_i10_hw	113		B315 interference noise 10
a50_i10_hw	155		B315 interference noise amplitude 10
a50_n50	143		B315 amplitude 50 and noise 50

It should be noted from Table 3 that for the autocorrelation case the pedestal of the auto-correlation peak is very low, signifying a very narrow peak. However, for the images that are significantly different than the template, the pedestal is high. The noisy images produce a correlation with a wider peak or many false peaks, which is less than the absolute maximum, but greater than the noise-free case. Analyzing Table 3, a post-processor could be designed to reject a correlation peak with a pedestal above 160. This ensures that it will accept all similar class images but reject all of the out-of-class images. But noticing that the real images are not as noisy, we lowered the threshold to 100 so that most of the noisy images were rejected. This ensures that when the beam pattern starts to change the correlation peak width will also change and be detected. This allows us to change the templates to accommodate the new reflection pattern. It is possible to incorporate the peak pedestal measurement into the uncertainty. As the peak broadens the uncertainty increases. For example, if peak width is less than 100, scale by 100; above 100, scale by 50; between 120 to 160, scale by 30; etc. This scaled factor can be multiplied with the calculated uncertainty. Thus as the peak width increases the more likely it is that the image will differ from the template. Another application of this post-processing approach is to switch between multiple algorithms in case the image is correct but significantly distorted for some other reason.

6. CONCLUSIONS

To make the algorithm more accurate with a constantly updated template, it is possible to switch to a tracking algorithm [12] where it uses the current image as the template. It used the first template to find the position of the current image template. Then this is used in the subsequent iterations to find the next image positions. The optimization of this new AMPOF filter [7] is a multivariable design optimization problem. In the design of this particular AMPOF we had four different variables to optimize. We used the radial standard deviation as the function to be optimized. Other objective functions to optimize include the correlation peak, variation in the correlation peaks [7], etc. It is possible to extend the post-processing concepts and design a neural network, which takes multiple parameters as inputs and optimizes the weights on the different parameters. If the search space to be detected becomes highly nonlinear then the complex-valued neural network may be used, which can have highly nonlinear boundaries [15].

ACKNOWLEDGEMENT

The authors acknowledge discussions with Erlan Bliss and Scott Burkhart about the KDP alignment requirements and Paul Van Arsdall for useful feedback about the paper. This work was performed under the auspices of the U.S. Department of Energy by the University of California, Lawrence Livermore Laboratory under contract No. W-7405-Eng-48.

REFERENCES

1. E. Moses, et al., "The National Ignition Facility: Status and Plans for Laser Fusion and High-Energy-Density Experimental Studies", *Fusion Science and Technology*, V. 43, p. 420, May 2003.
2. M. Rahman, A. A. S. Awwal, and K. Gudmundsson, "Composite Filters for Search Time Reduction for 3D Model Based Object Recognition," *Photonic Devices and Algorithms for Computing V*, K.M. Iftakharuddin and A. A. S. Awwal, Editors, Proc. of SPIE, Vol. 4201, 2003.
3. A. A. S. Awwal, M. A. Karim, and S. R. Jahan, "Improved Correlation Discrimination Using an Amplitude-Modulated Phase-Only Filter," *Applied Optics*, Vol. 29, pp. 233-236, 1990.
4. VanderLugt, "Signal Detection by Complex Spatial Filtering", *IEEE Trans. Inf. Theory* IT-10, 139-145 (1964).
5. J. L. Horner and J. Leger, "Pattern Recognition With Binary Phase-Only Filters", *Appl. Opt.* 24, 609-611 (1985).
6. M. A. Karim and A. A. S. Awwal, "Optical Computing: An Introduction", John Wiley, New York, NY, 1992.
7. K. M. Iftakharuddin, M. A. Karim, and A. A. S. Awwal, "Optimization of Amplitude Modulated Inverse Filter", *Mathematical and Computer Modeling*, Vol. 24, pp. 103-112, 1996.
8. K. M. Iftakharuddin, M. A. Karim, P. W. Elloe, and A. A. S. Awwal, "Discretized Amplitude-Modulated Phase-Only filter", *Optics and Laser Technology*, Vol. 28, pp. 93-100, 1996.
9. Personal communications with Paul Wegner at NIF.
10. J. P. Holman (in collaboration with W. J. Gajda), *Experimental Methods for Engineers*, Chapter 3–11, McGraw-Hill Book Co., 3rd edition, 1978.
11. James V. Beck and Kenneth J. Arnold, *Parameter Estimation in Engineering and Science*, John Wiley & Sons, New York, 1977.
12. Karl S. Gudmundsson, and A. A. S. Awwal, "Sub-Imaging Technique to Improve POF Search Capability", *Applied Optics*, Vol. 42, pp. 4709-4717, 2003.
13. A. A. S. Awwal and H. E. Michel, "Enhancing the Discrimination Capability of Phase Only Filter", *Asian Journal of Physics*, Vol. 8, pp. 381-384, 1999.
14. F. Ahmed, A. A. S. Awwal and M. A. Karim, "Improved Recognition Performance With Synthetic Correlator," *Microwave and Optical Technology Letter*, Vol. 14, pp. 274-278, 1997.
15. H. E. Michel, and A. A. S. Awwal, "Enhanced Artificial Neural Networks Using Complex-Numbers", 1999 International Joint Conference on Neural Networks. See also Howard E. Michel, Enhanced Artificial Neural Network Performance using Multidimensional Complex Numbers, Ph.D. thesis, Wright State University, 1999.